Naval Research Laboratory

Washington, DC 20375-5320

NRL/MR/5651--15-9624

W-Band Technology and Techniques for Analog Millimeter-Wave Photonics

Vincent J. Urick
Christopher S. Sunderman
John F. Diehl

Photonics Technology Branch
Optical Sciences Division

Nicholas D. Peterson

Naval Air Warfare Center
Aircraft Division
Patuxent River, Maryland

August 19, 2015

REPORT DOCUMENTATION PAGE

Form Approved
OMB No. 0704-0188

1. REPORT DATE *(DD-MM-YYYY)*	**2. REPORT TYPE**	**3. DATES COVERED** *(From - To)*
19-08-2015	Memorandum	01 November 2014 – 11 March 2015

4. TITLE AND SUBTITLE

W-Band Technology and Techniques for Analog Millimeter-Wave Photonics

5a. CONTRACT NUMBER

5b. GRANT NUMBER

5c. PROGRAM ELEMENT NUMBER
62271N

6. AUTHOR(S)

Vincent J. Urick, Christopher S. Sunderman, John F. Diehl,
and Nicholas D. Peterson*

5d. PROJECT NUMBER

5e. TASK NUMBER
EW-271-03

5f. WORK UNIT NUMBER
6582

7. PERFORMING ORGANIZATION NAME(S) AND ADDRESS(ES)

Naval Research Laboratory, Code 5651
4555 Overlook Avenue, SW
Washington, DC 20375-5320

8. PERFORMING ORGANIZATION REPORT NUMBER

NRL/MR/5651--15-9624

9. SPONSORING / MONITORING AGENCY NAME(S) AND ADDRESS(ES)

Office of Naval Research
One Liberty Center
875 North Randolph Street, Suite 1425
Arlington, VA 22203-1995

10. SPONSOR / MONITOR'S ACRONYM(S)

ONR

11. SPONSOR / MONITOR'S REPORT NUMBER(S)

12. DISTRIBUTION / AVAILABILITY STATEMENT

Approved for public release; distribution is unlimited.

13. SUPPLEMENTARY NOTES

*Naval Air Warfare Center Aircraft Division, 22347 Cedar Point Road, Unit 6, Bldg. 2185, Rm. 3250, Patuxent River, MD 20670-1161

14. ABSTRACT

This report provides an overview of the available technology and standard techniques for millimeter-wave photonics at frequencies up to 110 GHz. Measured data for commercial electro-optic phase modulators, electro-optic intensity modulators, p-i-n photodiodes and waveguide photodetectors are presented. These data are analyzed utilizing typical link gain equations. Multiplexing techniques, which are not trivial with W-Band modulation, are described.

15. SUBJECT TERMS

Fiber optics
Analog photonics
Millimeter Wave
W-Band

16. SECURITY CLASSIFICATION OF:			**17. LIMITATION OF ABSTRACT**	**18. NUMBER OF PAGES**	**19a. NAME OF RESPONSIBLE PERSON**
a. REPORT	**b. ABSTRACT**	**c. THIS PAGE**			Vincent J. Urick
Unclassified Unlimited	Unclassified Unlimited	Unclassified Unlimited	Unclassified Unlimited	20	**19b. TELEPHONE NUMBER** *(include area code)* (202) 767-9352

Standard Form 298 (Rev. 8-98)
Prescribed by ANSI Std. Z39.18

TABLE OF CONTENTS

EXECUTIVE SUMMARY

This report provides an overview of the available technology and standard techniques for millimeter-wave photonics at frequencies up to 110 GHz. Measured data for commercial electro-optic phase modulators, electro-optic intensity modulators, p-i-n photodiodes and waveguide photodetectors are presented. These data are analyzed utilizing typical link gain equations. Multiplexing techniques, which are not trivial with W-Band modulation, are described.

W-BAND TECHNOLOGY AND TECHNIQUES FOR ANALOG MILLIMETER-WAVE PHOTONICS

1 INTRODUCTION

Analog photonics is an applied field with a rich history [1] that finds utility in numerous areas. An inherent advantage of photonics over electronics is the available bandwidth of the former, allowing for frequency coverage from near DC to well into the millimeter wave and even sub-THz rages. A number of photonic approaches have been considered for usage at millimeter-wave frequencies, including bulk fiber-optic and integrated technologies [2-4]. Whether the millimeter-wave application is associated with wireless links [5-7], radio astronomy [8], or military systems, the main components that determine the performance are the electrical-to-optical (E/O) and optical-to-electrical (O/E) conversion mechanisms. This report provides measurement data for the state-of-the-art millimeter wave electro-optical components with frequency coverage up to 110 GHz. A terse review of the most prevalent architectures for such applications is provided in §2. Also included there is a brief, but standalone, mathematical description that demonstrates the most important component parameters. Measurements of such parameters are provided in §3 for $LiNbO_3$ phase and intensity modulators, and waveguide and surface illuminated photodetectors. Highlights of various techniques to overcome present-day component limitations are provided in §4, leaving much for the interested reader to further research. Finally, a short outlook is given in §5.

Manuscript approved March 13, 2015.

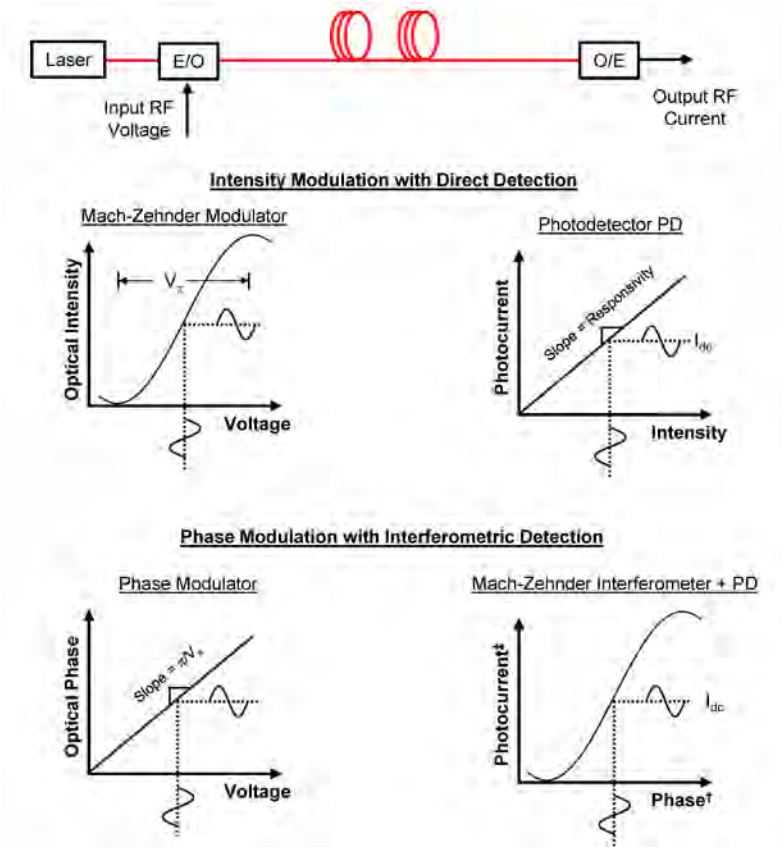

Fig. 1. Block diagram for a fiber-optic link having electrical-to-optical (E/O) and optical-to-electrical (O/E) conversion stages. In the case of intensity modulation, optical phase modulation is converted directly to optical intensity modulation in an integrated Mach-Zehnder modulator (MZM) on the E/O side of the link. A phase modulated link achieves this conversion on the back end of the link as part of the O/E stage.
†Strictly, this axis is the input phase differential, $\phi(t)-\phi(t-\tau)$ where τ is the differential delay between the two arms in the interferometer.
‡Shown for continuous RF waveform at peak response. In general, the RF response depends on the time-domain waveform of the RF signal and its relation to τ.

2 BASIC LINK CONFIGURATIONS

A simple photonic link is shown at the top of Fig. 1. A laser is modulated by an RF signal in an electrical-to-optical (E/O) conversion block. There are many methods that can be utilized for this modulation [1]; the best candidate for millimeter applications remains $LiNbO_3$, an electro-optic crystal. When a voltage is applied to such a crystal, the optical index of refraction is linearly shifted, thus providing a mechanism to encode RF signals onto the laser's phase. Such phase modulation cannot be directly detected by a stand-alone photodetector because they are sensitive to intensity modulation only. Therefore, some technique must be employed to convert optical phase modulation into intensity modulation such that the signal can be recovered in the RF domain. The most common is a Mach-Zehnder modulator (MZM), an integrated interferomter that exhibits as sinusoidal transfer function as shown in Fig. 1. The output of such a device can then undergo optical-to-electrical (O/E) conversion with a singular photodetector. On the other hand, a passive phase modulator can also be employed for the E/O stage. There are many methods to convert optical phase modulation into intensity modulation (see Chapter 7 in [1]);

here, we restrict the analysis to a path-imblanced Mach-Zehnder interferometer (MZI). The ideal actions of such a link are shown in the bottom of Fig. 1. A linear phase modulation is applied on the E/O side of the link, which is then converted to intensity modulation via the sinusoidal transfer function of the MZI. A photodetector(s) at the output of the MZI then converts the signal back into the electrical domain. Thus, the E/O stage is an MZI with a photodetector in this case. As can be seen, this process is a reversal of that for the MZM-based link but similar in many regards.

A complete analysis of the links noted in Fig. 1 is provided in Chapters 6 and 7 of [1]. Here a brief review is provided for completeness and in order to convey the important component parameters. A scalar field transfer matrix can be written for the IMDD case as

$$\begin{bmatrix} E_1(t) \\ E_2(t) \end{bmatrix} = \frac{\sqrt{\alpha}}{2} \begin{bmatrix} 1 & i \\ i & 1 \end{bmatrix} \begin{bmatrix} e^{i\phi(t)/2} & 0 \\ 0 & e^{-i\phi(t)/2} \end{bmatrix} \begin{bmatrix} 1 & i \\ i & 1 \end{bmatrix} \begin{bmatrix} E_0(t) \\ 0 \end{bmatrix}, \tag{1}$$

where $E_0(t) = \kappa\sqrt{2P}e^{i\omega t}$ is the field at the output of the laser with P being the average laser power at angular frequency ω. The constant κ is introduced such that $P = E_0^* E_0 \big/ \left(2\kappa^2\right)$. The term $\phi(t)$ is the optical phase shift induced by the voltage applied to the MZM. For the purposes here, we consider a DC bias voltage and a single sinusoidal RF signal such that $\phi(t) = \pi\left(V_{\mathrm{dc}}/V_{\pi,\mathrm{dc}}\right) + \pi\left(V/V_\pi\right)\sin(\Omega t)$, where V_{dc} is the applied bias, V is the peak voltage of the input signal at angular frequency Ω, and V_π is the frequency-dependent voltage required to achieve π optical phase shift. Finally, the term α in (1) accounts for optical power loss in the link. Using the same definitions, a transfer matrix for the phase modulated link can be written as

$$\begin{bmatrix} E_1(t) \\ E_2(t) \end{bmatrix} = \frac{\sqrt{\alpha}}{2} \begin{bmatrix} 1 & i \\ i & 1 \end{bmatrix} \begin{bmatrix} \Gamma(\tau) & 0 \\ 0 & 1 \end{bmatrix} \begin{bmatrix} 1 & i \\ i & 1 \end{bmatrix} \begin{bmatrix} e^{i\phi(t)}E_0(t) \\ 0 \end{bmatrix}, \tag{2}$$

where $\Gamma(\tau)$ operates on a time-dependent field as $\Gamma(\tau)E(t) = E(t-\tau)$, with τ being the differential time delay between the two arms in the MZI. Now, detection of the fields E_1 and E_2 in (1) and (2) produces photocurrents of the form [9]

$$\begin{aligned} I_{1,2}(t) = {} & I_{\mathrm{dc,q}} \mp \cos(\theta) I_{\mathrm{dc,q}} J_0(x) \\ & \mp 2\cos(\theta) I_{\mathrm{dc,q}} \sum_{k=1}^{\infty} J_{2k}(x)\cos(2k\Omega t) \\ & \pm 2\sin(\theta) I_{\mathrm{dc,q}} \sum_{m=0}^{\infty} J_{2m+1}(x)\sin\left[(2m+1)\Omega t\right] \end{aligned} \tag{3}$$

where $I_{\mathrm{dc,q}}$ is the DC photocurrent when θ is an odd-integer multiple of $\pi/2$ (quadrature condition) and J is a Bessel function of the first kind. The parameters θ and x take on the values $\theta_{\mathrm{I}} = \pi V_{\mathrm{dc}}/V_{\pi,\mathrm{dc}}$, $\theta_\Phi = \omega\tau$, $x_{\mathrm{I}} = \pi V/V_\pi$ and $x_\Phi = 2\pi V \sin(\pi f \tau)/V_\pi$, where "I" indicates intensity modulation and "Φ" phase modulation. It should be noted that (3) is the ideal photocurrent not including photodetector effects; the photodiode frequency response is handled below in (4) and (5). Finally, (3) excludes a constant phase shift in the case of phase modulation that is unimportant here but can arise in more advanced applications (see [10]).

The primary measurement results utilized in the next section are the small-signal RF gain, obtained from a vector network analyzer (VNA). Expressions for these values can be obtained from (3) as

$$g_{\mathrm{I}} = \frac{I_{\mathrm{dc}}^2}{V_\pi^2}\pi^2 R_{\mathrm{i}} R_{\mathrm{o}} \left|H_{\mathrm{pd}}\right|^2 \sin^2\left(\theta_{\mathrm{I}}\right) \tag{4}$$

$$g_{\Phi} = 4\frac{I_{\mathrm{dc}}^2}{V_\pi^2}\pi^2 R_{\mathrm{i}} R_{\mathrm{o}} \left|H_{\mathrm{pd}}\right|^2 \sin^2\left(\pi f \tau\right)\sin^2\left(\theta_{\Phi}\right), \tag{5}$$

where R_{i} and R_{o} are the resistances at the link input and output, respectively, and H_{pd} is the Fourier transform of the photodetector circuit impulse response. With the assumption that the quadrature condition is precisely achieved and that impedances are matched across all frequencies ($R_{\mathrm{i}} = R_{\mathrm{o}}$ = constant)[1], the RF response of the link is determined by I_{dc}, V_π and H_{pd} (and τ for the phase modulated case). The I_{dc} term is frequency independent. Therefore with the above assumptions, degradations in S_{21} as a function of frequency are governed by V_π and H_{pd}.

[1] Given this assumption, degradations to the frequency response due to impedance mismatch are absorbed into V_π and H_{pd}.

3 COMPONENT TECHNOLOGY

The majority of the data presented in this section were obtained with a calibrated vector network analyzer (VNA). The instrument was an Agilent Technologies PNA-X N5247A mainframe with 67 GHz of range coupled to N5260 extender modules for the 110 GHz data. The links were arranged for a standard four-port measurement, with the VNA source (Port 1) input to the external modulator and the photodetector output coupled to Port 2 on the VNA. The resulting data are presented at the end of this section with a description of the links in the following.

Shown in Fig. 2 are the measured gain and reflection coefficient from the input for a link employing an MZM and singular photodetector. The MZM was a $LiNbO_3$ device with a side-fed 1.0-mm input, EOSPACE M/N AZ-DV5-100-PFA-PFA-UWB-SNR613 and S/N 329226. The photodetector was of the waveguide variety, a U^2T M/N XPDV4120R-WP-FP with S/N 89775 B9W.0163. For the data in Fig. 2, the MZM was biased at quadrature and the received photocurrent was 3.75 mA. As can be seen, there are three nulls in the frequency response and these are all attributed to the MZM. The normalized photodetector response is shown in Fig. 3, a digitized version of the curve provided by the manufacturer of the device. A two-piece, fourth-order polynomial curve was fit to these data such that the photodetector response could be removed from the link response in Fig. 2. The results of this practice are shown in Fig. 3, where the plot for the entire link and that with the photodetector contribution removed are depicted. As can be seen there, the photodetector does not degrade the response below 67 GHz. The black curve in Fig. 3 therefore constitutes a measurement of (4) with $\left|H_{\mathrm{pd}}\right|^2 = 1$ and $\sin^2\left(\theta_{\mathrm{I}}\right) = 1$. Assuming that $R_{\mathrm{i}} = R_{\mathrm{o}} = 50\ \Omega$ and inserting $I_{\mathrm{dc}} = 3.75$ mA, V_π can be plotted as a function of frequency as in Fig. 5. Note that this is an effective V_π, capturing all of the imperfections of the packaged MZM, and should not necessarily be tied directly to the crystal's electro-optic coefficient. The same MZM was being reevaluated at a later date, the results of which are shown in Fig. 6. The parameters and setup are identical to the previous measurement with the exception that $I_{\mathrm{dc}} = 2$ mA. As can be seen a significant degradation in the response was observed, which has been attributed to the electrode mount to the crystal. No notable events occurred with the MZM between measurements, highlighting the potential delicacy of millimeter-wave electrodes. The unit is presently out for evaluation and possible repair by the manufacturer.

Measured data for three $LiNbO_3$ phase modulators are shown in Figs. 7 and 8. The three devices are labeled as follows: PM1: EOSPACE PM-WWtop-PFA-PFA-NRL with S/N 329612, PM2: EOSPACE PM-DV5-PFA-UWB-SNR613 with S/N 329016, and PM3: Phase Sensitive Innovations packaged prototype labeled LM05. For all three modulators, an MZI with $\tau = 375$ ps biased at quadrature was employed with a single photodetector (U^2T M/N XPDV4120R-WP-FP with S/N 89775 B9W.0163) operating at $I_{\mathrm{dc}} = 2$ mA. The data in Fig. 7 show the link response without any corrections. The periodic nature as described by (5) is evident. Figure 8 shows points from Fig. 7 for each phase modulator spaced every 2.67 GHz ($1/\tau$) at the peak response points where $\sin^2\left(\theta_\Phi\right) = 1$, and with the photodetector response removed as described above.

Six millimeter-wave photodetectors were also evaluated as shown in Fig. 9 and 10. Four surface-illuminated devices and two waveguide devices were tested. The four surface-illuminated photodiodes were all from Discovery Semiconductor with model numbers DSC20 (S/N 210001), DSC20H (S/N 220369), DSC10H (S/N 20436), and DSC10ER (S/N 100198). The two waveguide photodetectors were manufactured by U^2T, model numbers XPDV3120R (S/N 132373 B912849) and XPDV4120R-WP-FP (S/N 89775 B9W.0163). For all the data in Fig. 9, PM1 and the 375-ps MZI were used, with each photodetector adjusted to $I_{\mathrm{dc}} = 2$ mA. The response of the photodetectors can be compared by using the PM1 data in Fig. 8 along with (5)—this method is redundant for the 110 GHz photodetector. The results, assuming that $R_{\mathrm{i}} = R_{\mathrm{o}} = 50\ \Omega$, are shown in Fig. 10.

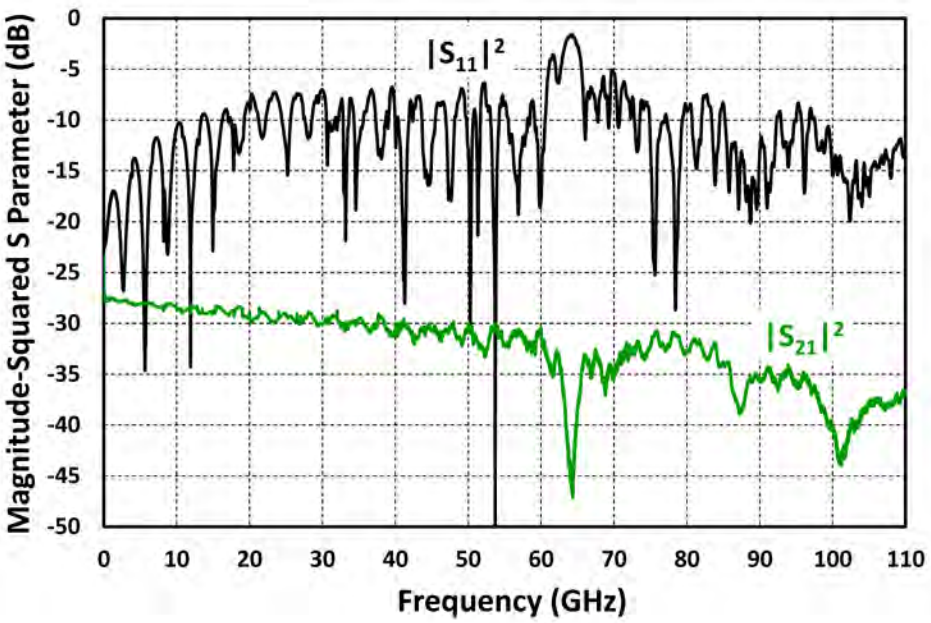

Fig. 2. Measured RF gain ($|S_{21}|^2$) and input reflection coefficient ($|S_{11}|^2$) for an intensity modulation direct detection link utilizing an EOSPACE MZM (S/N 329226) and a U^{2}T photodetector (S/N 89775 B9W.0163). The average photocurrent was I_{dc} = 3.75 mA.

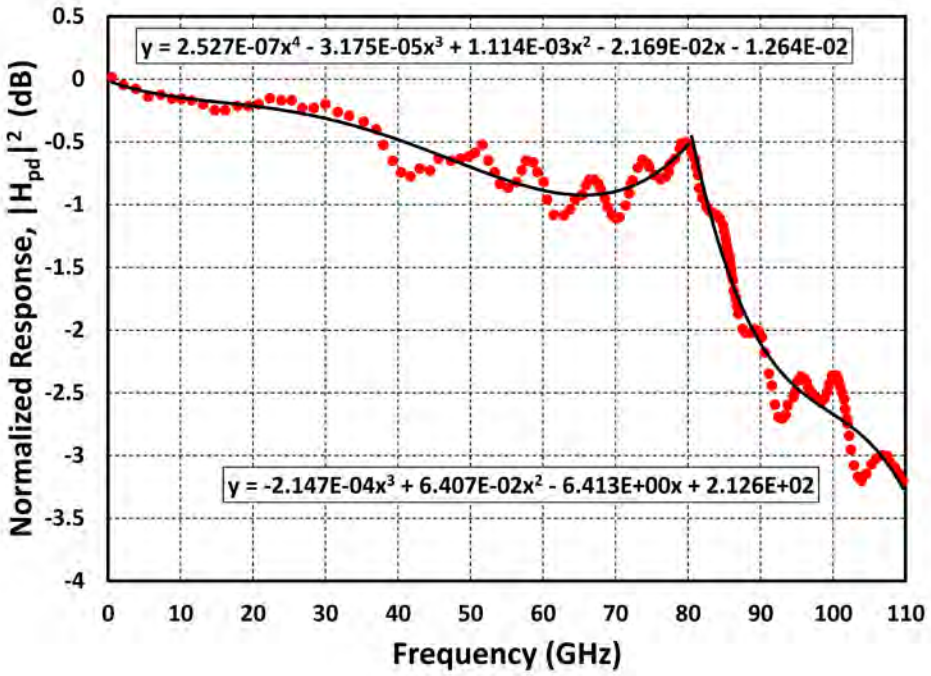

Fig. 3. Response for U^{2}T photodetector (S/N 89775 B9W.0163) used to isolate modulator responses. The red circles are data provided by the vendor. Lines designate a piece-wise polynomial employed to calculate the response as a function of frequency.

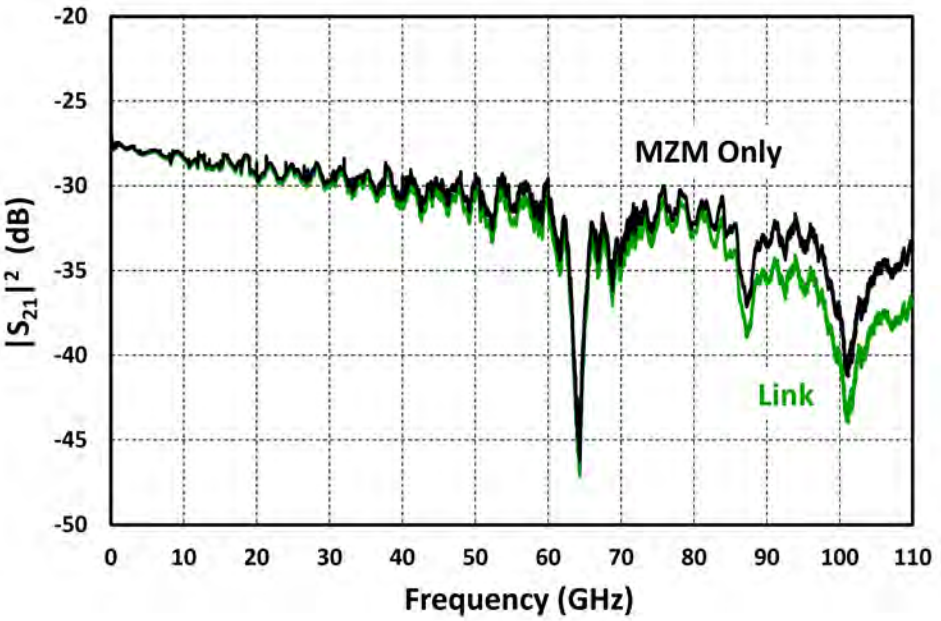

Fig. 4. Measured responses for an IMDD link repeated from Fig. 2 (green) and the response of the MZM only (black) with contributions from the photodetector removed, as obtained utilizing the data in Fig. 3.

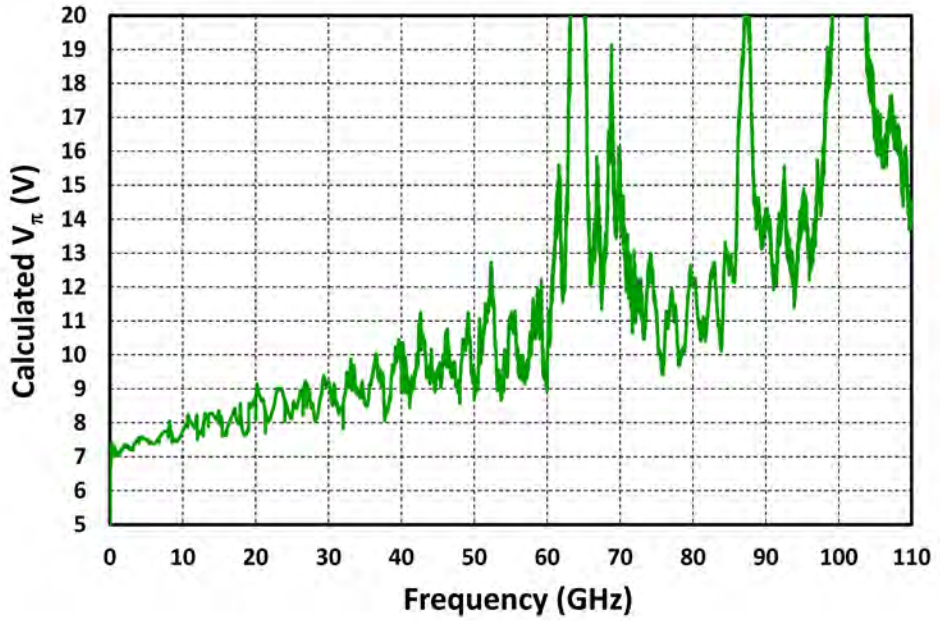

Fig. 5. Calculated half-wave voltage for the MZM in Fig. 4, obtained by applying (4) to the black curve.

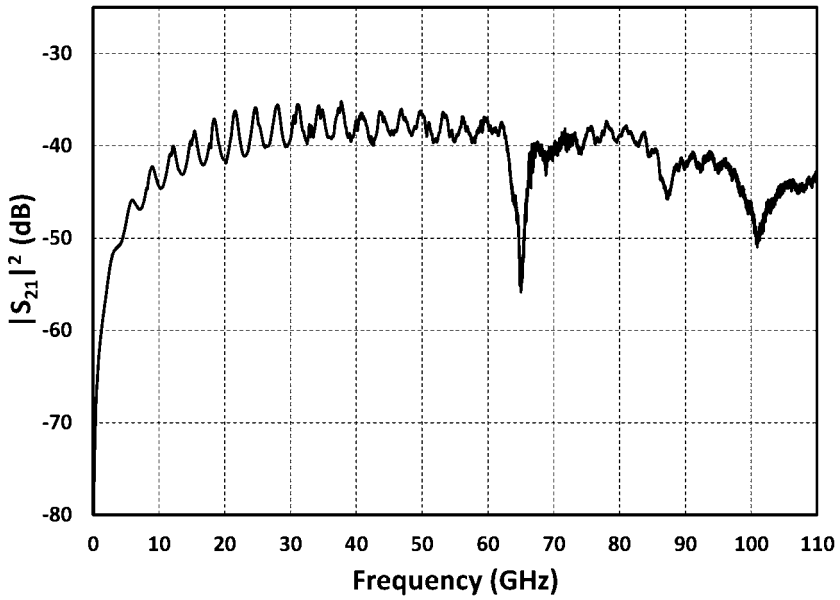

Fig. 6. Measured response using the same components as in Fig. 2 but at a later date and with I_{dc} = 2mA. The significant degradation in the response is attributed to the MZM.

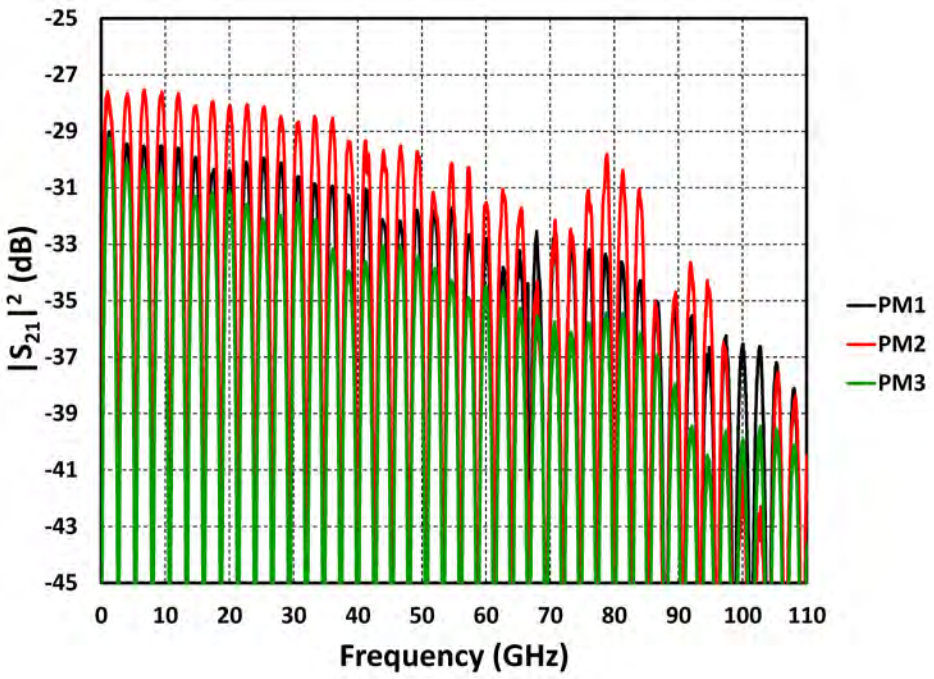

Fig. 7. Measured response of phase-modulated links utilizing an MZI having τ = 375 ps. The three devices shown are an EOSPACE S/N 329612 (PM1), EOSPACE S/N 329016 (PM2) and Phase Sensitive Innovations M/N LM05 (PM3). For these data, a U^2T photodetector (S/N 89775 B9W.0163) operated at I_{dc} = 2 mA was employed.

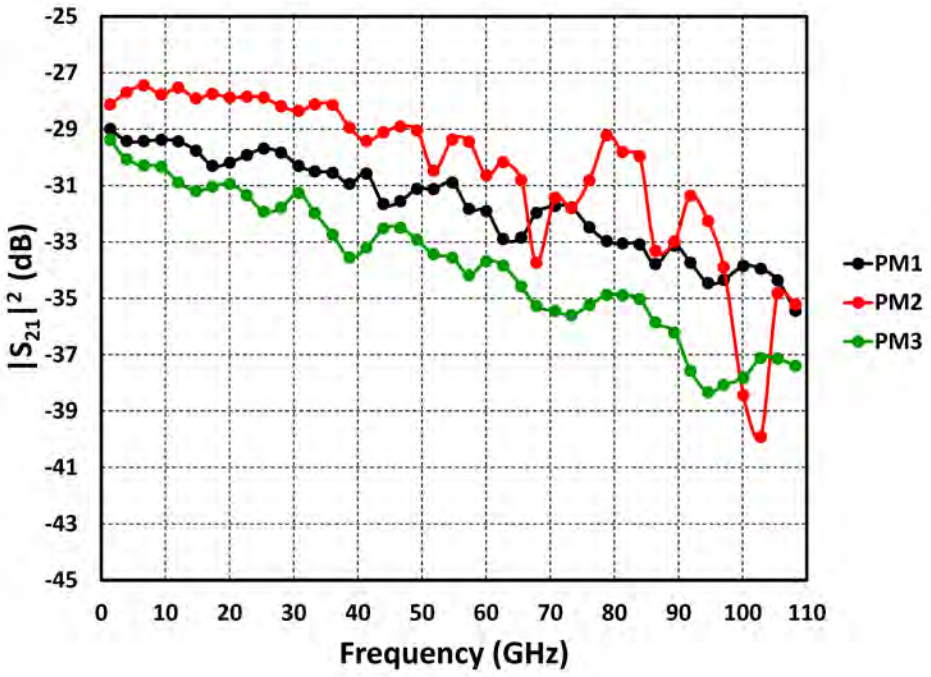

Fig. 8. Responses for the phase modulators in Fig. 7, with data points taken at the peaks of the MZI filter function and with the response of the photodetector removed using Fig. 3.

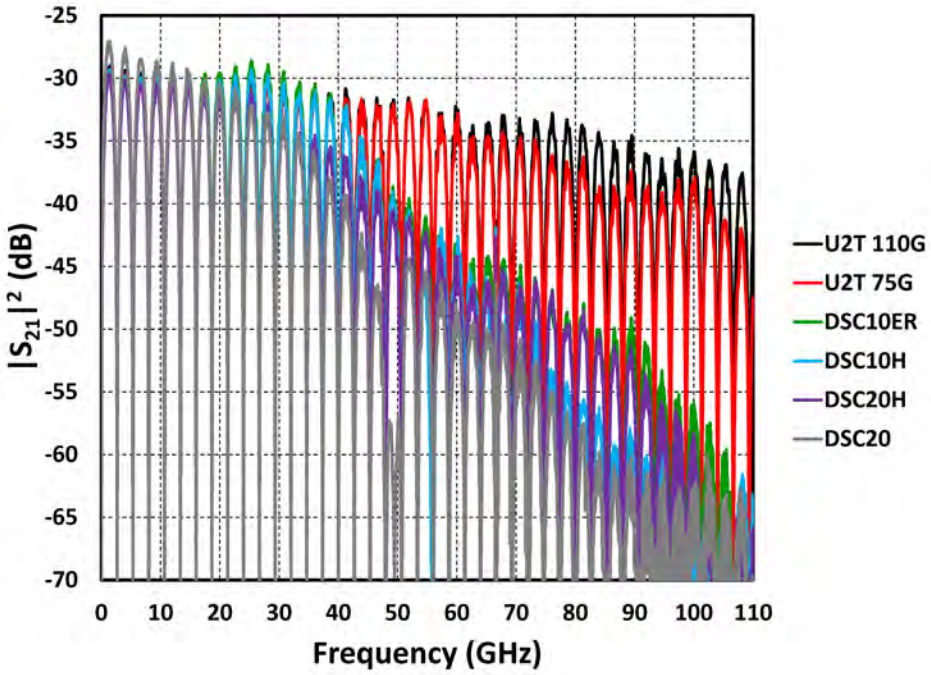

Fig. 9. Measured data for phase modulated links employing various millimeter-wave photodetectors. The same modulator was used for all curves, EOSPACE S/N 329612, and I_{dc} = 2 mA for each detector. Data are shown for U^{2}T S/Ns 89775 B9W.0163 (U2T 110G) and 132373 B912849 (U2T 75G), and Discovery Semiconductor S/Ns 100198 (DSC10ER), 20436 (DSC10H), 220369 (DSC20H) and 210001 (DSC20).

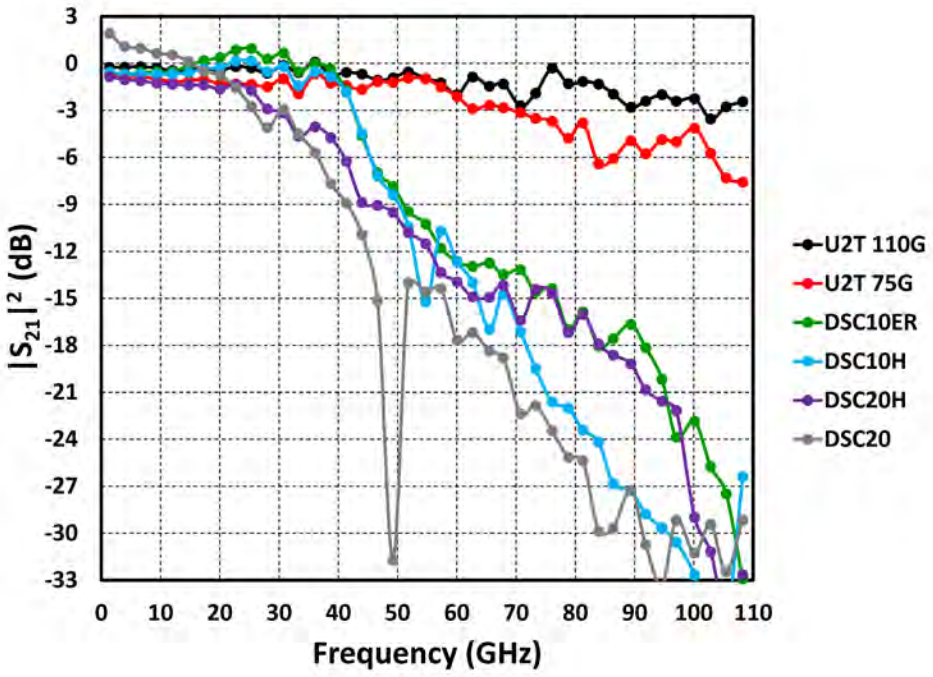

Fig. 10. Data for the photodetectors in Fig. 9 with the phase modulator response removed by using the data in Fig. 8 for PM1.

TABLE 1: FIVE-CHANNEL WDM GRID FOR W-BAND APPLICATIONS

Frequency (THz)	Wavelength (nm)
191.4	1566.31
192.4	1558.17
193.4	1550.12
194.4	1542.14
195.4	1534.25

4 MULTIPLEXING TECHNIQUES

There are a number of multiplexing techniques that are employed for industrial communications, where independent signals can be encoded onto various different properties of light in order to increase the capacity of long-haul fiber-optic cables. Reviews of the various techniques have been presented in numerous publications; two complimentary works are [11] and [12]. The most widespread is what is known as wavelength division multiplexing (WDM), a technique that dates to the beginning of modern fiber-optic networks [13]. As an example, many fiber-to-the-premises (FTTP) architectures employ 1550- and 1490-nm downlinks with 1310-nm uplinks [14]. Much finer channel spacing is used in dense WDM, or DWDM, where the frequency spacing can be as small as 12.5 GHz [15]. When the channel spacing is on the order of the data rate, it is sometimes referred to as frequency division multiplexing (FDM). Orthogonal FDM (OFDM) is a technique where an information stream is subdivided into lower rate sub-channels [16]. Both FDM and OFDM require precise control of the optical channels. A technique similar to OFDM but implemented in the time domain is time division multiplexing (TDM) [17]. A single optical signal can be modulated by separate RF subcarriers each carrying independent information, a technique termed sub-carrier multiplexing long ago [18-20]. Two orthogonal polarizations of single optical wavelength can be modulated separately in polarization division multiplexing (PDM) [21]. Optical code division multiple access (CDMA) is a technique where coding, or signature sequences, are employed on spectrally and temporally overlapping signals that can be separated with correlation techniques and matched filtering [22-24]. Another option is mode-division multiplexing [25], where separate modes in a multi-mode waveguide can carry different information. Alternatively, what has come to be known as space division multiplexing (SDM) [26] utilizes separate single modes in photonic crystal fibers [27] or multicore fibers [28].

There are cases in analog photonic applications where the same RF signal requires distribution to different physical locations and/or processing through separate optical paths. In these cases, the first considerations should be to leverage the existing techniques described above. Previously demonstrated systems for analog signals include WDM [29, 30], tapered fibers [31,32] and multicore fibers [33], among others. For the purposes of distributing a single RF signal, WDM is the most straightforward multiplexing technique to implement. However, with modulation frequencies reaching 100 GHz, WDM is not a trivial endeavor to undertake. For example, modulation to the top of W-Band at 110 GHz requires 220 GHz of optical bandwidth per channel (with no margin between channels). That is, the dual-sideband nature of either phase or intensity modulation requires an optical bandwidth twice the maximum modulation frequency. Therefore, "Conventional" C-Band optical components (1530-1565 nm or 195.9-191.6 THz) support about 18 W-Band channels with a 10-GHz guard band on each side of the carrier. Furthermore, this type of architecture cannot be implemented with standard 200-GHz WDM filters, which are readily available. A 200-GHz Arrayed Waveguide Grating (AWG), which is commonly used for WDM applications, cannot be used in a W-Band implementation without having RF spectral overlap between channels. However, optical bandsplitters, typically used in an add/drop filter configuration, can be utilized. For example, there are commercially available

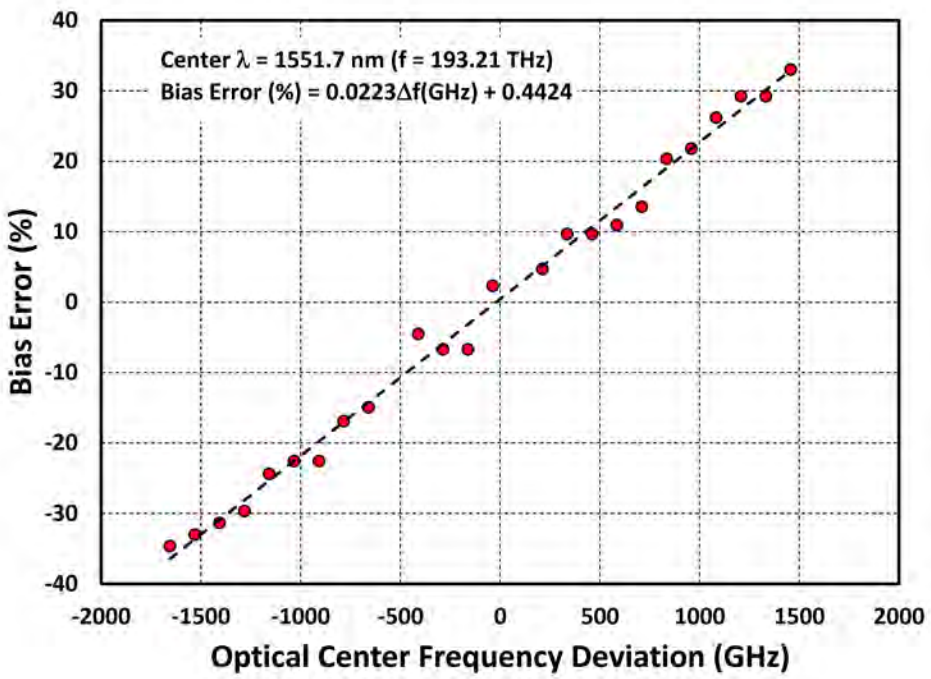

Fig. 11. Measured (symbols) deviation from quadrature for a 110-GHz MZM (EOSPACE S/N 329226).

components with adequately large passbands of ±387.5 GHz and ±487.5 GHz with a flat top response and fairly low dispersion. As simple exercise, a five-channel grid tailored to such filters is shown in Table 1, which spans 2 THz on either side of the center channel.

Another issue with W-Band WDM addressed with the data in Fig. 11 is the available bandwidth within the MZM transfer function (see Fig. 1). The quadrature bias condition can be uniquely achieved for only one wavelength, as can be seen in Fig. 11. Applying the trend in Fig. 11 to the grid in Table 1, it can be seen that the bias error on the two farthest channels from center are ±45° (±π/4). Now, by way of (4) this error in bias amounts to a 3-dB penalty in RF gain for the two distal channels. This may be able to be compensated for in some situations but could lead to problems in others. Another issue with MZM bias error is the generation of even-order distortion that is absent in an ideal quadrature-biased link. This can be seen in the form of (3) and is also detailed in [34]. Therefore, careful analysis must be conducted when considering such a wide bandwidth in multi-octave applications.

5 SUMMARY AND CONCLUSIONS

Analog photonic technologies into the W-Band (75-110 GHz) are now commercially available. The required optical components such as lasers, fiber, couplers, filters, amplifiers and switches are for the most part the same that have been traditionally employed in microwave photonics and/or industrial telecommunications for decades. However, the E/O (modulators) and O/E (photodetectors) components are limited to a few vendors and lack a high-volume application. The leading devices have been characterized in this report. The performance is acceptable for some applications but may be lacking in others, such as high sensitivity links requiring low noise figure. There is room for improvement, particularly on the E/O side, but major advances would require significant investment of resources. Multiplexing techniques and other innovative architectural methods may provide solutions to mitigate the component limitations. Some of the former have been outlined here. Some architectural techniques might include cascaded approaches on the E/O side [35,36] and/or the O/E side [37]. Ultimately, these types of approaches need to be evaluated on a case-by-case basis, where system requirements will determine the possible photonic designs. In any event, the data provided in this report provide a starting point for the innovative photonic system designer to address millimeter-wave capabilities.

REFERENCES

[1] V. J. Urick, J. D. McKinney, and K. J. Williams, *Fundamentals of Microwave Photonics*, Wiley, 2015.

[2] B. Vidal, T. Nagatsuma, N. J. Gomes, and T. E. Darcie, "Photonic technologies for millimeter- and submillimeter-wave signals," *Advances in Optical Technologies*, 925065, 2012.

[3] A. J. Seeds, M. J. Fice, K. Balakier, M. Natrell, O. Mitrofanov, M. Lamponi, M. Chtioui, F. van Dijk, M. Pepper, G. Aeppli, A. G. Davies, P. Dean, E. Linfield, and C. C. Renaud, "Coherent terahertz photonics," *Opt. Exp.*, vol. 21, no. 19, pp. 22988-23000, 2013.

[4] G. Carpintero, K. Balakier, Z. Yang, R. C. Guzman, A. Corradi, A. Jimenez, G. Kervella, M. J. Fice, M. Lamponi, M. Chitoui, F. van Dijk, C. C. Renaud, A. Wonfor, E. A. J. M. Bente, R. V. Penty, I. H. White, and A. J. Seeds, "Microwave photonic integrated circuits for millimeter-wave wireless communications," *J. Lightwave Technol.*, vol. 32, no. 20, pp. 3495-3501, Oct. 2014.

[5] N. Kukutsu, A. Hirata, M. Yaita, K. Ajito, H. Takahashi, T. Kosugi, H. J. Song, A. Wakatsuki, Y. Muramoto, T. Nagatsuma, and Y. Kado, "Toward practical applications over 100 GHz," in *IEEE International Microwave Symp. Dig.*, pp. 1134-1137, 2010.

[6] G. K. Chang and C. Liu, "1-100 GHz microwave photonic link technologies for next-generation WiFi and 5G wireless communications," in *IEEE Topical Meeting on Microwave Photonics Dig.*, pp. 5-8, 2013.

[7] T. Nagatsuma, S. Horiguchi, Y. Minamikat, Y. Yoshimitzu, S. Hisatake, S. Kuwano, N. Yoshimoto, J. Terada, and H. Takahashi, "Terahertz wireless communications based on photonics technologies," *Opt. Exp.*, vol. 21, no. 20, pp. 23736-23747, 2013.

[8] B. Shillue, W. Grammer, C. Jacques, R. Brito, J. Meadows, J. Castro, Y. Masui, R. Treacy, and J. F. Cliche, "The ALMA photonic local oscillator system," *Proc. of SPIE*, 8452, 2012.

[9] M. N. Hutchinson, J. M. Singley, V. J. Urick, S. R. Harmon, J. D. McKinney, and N. J. Frigo, "Mitigation of photodiode induced even-order distortion in photonic links with predistortion modulation," *J. Lightwave Technol.*, vol. 32, no. 20, pp. 3885-3892, Oct. 2014.

[10] J. F Diehl, J. M. Singley, C. E. Sunderman, and V. J. Urick, "Microwave photonic delay line signal processing," submitted to *Appl. Opt.*, 2015.

[11] G. P. Agrawal, *Fiber-Optic Communication Systems*, Wiley, 2010.

[12] A, Brillant, *Digital and Analog Fiber Optic Communications for CATV and FTTx Applications*, SPIE and Wiley, 2008.

[13] C. A. Brackett, "Dense wavelength division multiplexing networks: principles and applications," *IEEE J. Selected Areas in Comm.*, vol. 8, no. 6, pp. 948-964, Aug. 1990.

[14] M. Abrams, P. C. Becker, Y. Fujimoto, V. O'Byrne, and D. Piehler, "FTTP deployments in the United States and Japan—equipment choices and service provider imperatives," *J. Lightwave Technol.*, vol. 23, no. 1, pp. 236-246, Jan. 2005.

[15] G. Keiser, *FTTX Concepts and Applications*, Wiley, 2006.

[16] I. B. Djordjevic and B. Vasic, "Orthogonal frequency division multiplexing for high-speed optical transmission," *Opt. Exp.*, vol. 14, no. 9, pp. 3767-3775, Apr. 2006.

[17] R. S. Tucker, G. Eisenstein, and S. K. Korotky, "Optical time-division multiplexing for very high bit-rate transmission," *J. Lightwave Technol.*, vol. 6, no. 11, pp. 1737-1749, Nov. 1988.

[18] T. E. Darice, "Subcarrier multiplexing for multiple-access lightwave networks," *J. Lightwave Technol.*, vol. 5, no. 8, pp. 1103-1110, Aug. 1987.

[19] T. E. Darcie, "Subcarrier multiplexing for lightwave networks and video distribution systems," *IEEE J. Selected Areas in Comm.*, vol. 8, no. 7, pp. 1240-1248, Sept. 1990.

[20] R. Hui, B. Zhu, R. Huang, C. T. Allen, K. R. Demarest, and D. Richards, "Subcarrier multiplexing for high-speed optical transmission," *J. Lightwave Technol.*, vol. 20, no. 3, pp. 417-427, Mar. 2002.

[21] P. M. Hill, R. Olshansky, and W. K. Burns, "Optical polarization division multiplexing at 4 Gb/s," *IEEE Photonics Technol. Lett.*, vol. 4, no. 5, pp. 500-502, May 1992.
[22] J. A. Salehi, "Code division multiple-access techniques in optical fiber networks—Part I: fundamental principles," *IEEE Trans. Comm.*, vol. 37, no. 8, pp. 824-833, Aug. 1989.
[23] K. Kitayama, "Code division multiplexing lightwave networks based upon optical code conversion," *IEEE J. Selected Areas in Comm.*, vol. 16, no. 7, pp. 1309-1319, Sept. 1998.
[24] P. R. Prucnal, *Optical Code Division Multiple Access: Fundamentals and Applications*, CRC Press, 2010.
[25] K. P. Ho and J. M. Kahn, "Linear propagation effects in mode-division multiplexing systems," *J. Lightwave Technol.*, vol. 32, no. 4, pp. 614-628, 2014.
[26] D. J. Richardson, J. M. Fini, and L. E. Nelson, "Space-division multiplexing in optical fibers," *Nature Photonics*, vol. 7, no. 5, pp. 354-362, May 2013.
[27] P. S. J. Russell, "Photonic-crystal fibers," *J. Lightwave Technol.*, vol. 24, no. 12, pp. 4729-4749, 2006.
[28] B. Zhu, J. M. Fini, M. F. Yan, X. Liu, S. Chandrasekhar, T. F. Taunay, M. Fishteyn, E. M. Monberg, and F. V. Dimarcello, "High-capacity space-division-multiplexed DWDM transmission using multicore fiber," *J. Lightwave Technol.*, vol. 30, no. 4, pp. 486-492, 2012.
[29] A. L. Campillo, E. E. Funk, D. A. Tulchinsky, J. L. Dexter, and K. J. Williams, "Phase performance of an eight-channel wavelength-division-multiplexed analog-delay line," *J. Lightwave Technol.*, vol. 22, no. 2, pp. 440-447, Feb. 2004.
[30] C. E. Sunderman and V. J. Urick, "Fiber-optic propagation effects in long-haul HF/VHF/UHF analog photonic links," NRL Memorandum Report, NRL/MR/5650-14-9537, Apr. 2014.
[31] C. A. Villarruel, C. A. McDermitt, and F. Bucholtz, "Microstructure fibre array for RF photonic signal processing applications," *Electron. Lett.*, vol. 42, no. 5, pp. 271-273, 2006.
[32] N. Mothe and P. D. Bin, "Multichannel microwave photonics signals summation device," *IEEE Photonics Technol. Lett.*, vol. 23, no. 3, pp. 140-142, 2011.
[33] I. Gasulla and J. Capmany, "Microwave photonics applications of multicore fibers," *IEEE Photonics J.*, vol. 4, no. 3, pp. 877-888, 2012.
[34] V. J. Urick, John F. Diehl, Meredith N. Draa, J. D. McKinney, and K. J. Williams, "Wideband Analog Photonic Links: Some Performance Limits and Considerations for Multi-Octave Implementations," *Proc. SPIE*, vol. 8259, 2012.
[35] V. J. Urick, J. D. McKinney, J. F. Diehl, J. M. Singley, and K. J. Williams, "Analog fiber-optic links employing cascaded phase modulation stages," *Microwave and Opt. Technol. Lett.*, vol. 54, no. 12, pp. 2797-2801, Dec. 2012.
[36] V. J. Urick, J. F. Diehl, C. E. Sunderman, J. D. McKinney, and K. J. Williams, "An optical technique for radio-frequency interference mitigation," submitted to *IEEE Photonics Technol. Lett.*, 18 Dec. 2014.
[37] V. J. Urick, A. S. Hastings, J. D. McKinney, C. Sunderman, J. F. Diehl, P. S. Devgan, K. Colladay, and K. J. Williams, "Photodiode linearity requirements for radio-frequency photonics and demonstration of increased performance using photodiode arrays," in *IEEE Topical Meeting on Microwave Photonics*, Gold Coast, Australia, pp. 86-89, Oct. 2008.